

An H76 α survey of galactic H II regions: electron temperature and element gradients

J. E. Wink¹, T. L. Wilson¹, and J. H. Bieging²

¹ Max-Planck-Institut für Radioastronomie, Auf dem Hügel 69, D-5300 Bonn 1, Federal Republic of Germany

² Radio Astronomy Laboratory, University of California, Berkeley, CA 94720, USA

Received April 14, accepted June 22, 1983

Summary. Measurements of the H76 α line and continuum data for 84 H II regions are used to obtain LTE Electron Temperatures, T_e^* . Comparisons with model calculations and other measurements show that T_e^* obtained from H76 α line and continuum data accurately represents the Electron Temperature, T_e . As with other surveys, there is a gradient in T_e : an unweighted, linear least squares fit gives $T_e = 4800 + 270 D_{GC}$, $4 \leq D_{GC} \leq 17$, where D_{GC} is the distance from the Galactic Center in kpc. The correlation coefficient is 0.70. There is no dependence of T_e on D_S , the distance from the Sun. At a given distance D_{GC} , the scatter in T_e from source to source barely exceeds the noise. *Our values of T_e for the nine H II regions in the Galactic Center are 2000 K larger than the value extrapolated from the disk ($D_{GC} \geq 4$ kpc).* If the value of T_e can be related to the (O/H) ratio, we find $\log(O/H) = -0.055 D_{GC} - 2.73$, for H II regions in the disk ($D_{GC} \geq 4$ kpc). The H II regions in the Galactic Center do not fit this relation: either the (O/H) ratio is close to the Solar System value, or the (O/H) ratio is larger and additional heat sources are present.

Key words: galactic radio sources – radio recombination lines – electron temperature – element abundances

1. Introduction

Although measurements of hydrogen radio recombination lines from galactic H II regions are reasonably straightforward, the interpretation of these results has undergone a number of revisions in the last 15 yr. The initial measurements for $\Delta n = 1$ transitions, made by Mezger and Höglund (1967) favored the simplest interpretation: in this picture, the line formation is an LTE process. The LTE Electron Temperature, T_e^* , which is calculated from the line-to-continuum intensity ratio, integrated over the line, is directly related to T_e , the actual Electron Temperature of the H II region. Measurements of the $\Delta n = 2$ transitions (Gardner and McGee, 1967) showed deviations from this simple LTE model. The situation was complicated because non-LTE line formation effects (Goldberg, 1966) would increase the peak line intensity, while collisional broadening (Griem, 1967) would lower it. A significant theoretical advance was the incorporation of both effects, in a self consistent way, for a variable density, constant electron temperature model by Brockelhurst and Seaton (1972). Lockman and Brown (1975) generalized this model

to include an increase of T_e in the H II region with distance from the exciting star.

At frequencies of ~ 5 GHz, the models predict a complex relation between T_e^* and T_e (see Brown et al., 1978). As found by a number of observers the values of T_e^* are nearly equal for a number of sources at 5 GHz (Churchwell et al., 1978) and 23 GHz (Wilson et al., 1979a). Seaton (1980) pointed out that the value of T_e^* seems to be close to T_e because the effects of stimulated emission and pressure broadening tend to balance. There is no guarantee that some deviations ($\sim 20\%$) could be present for some sources at some frequencies. (Walmsley, 1980; Shaver, 1980). All models, however, show that for typical emission measures recombination lines at frequencies higher than 14 GHz should exhibit no line masering. There is still a deviation from the LTE level population, but this does not depend on the source geometry, rather mainly on electron density. At high electron densities, ($N_e \geq 5 \cdot 10^3 \text{ cm}^{-3}$), the value of T_e and T_e^* should agree to within 10%. Since line and continuum obtained at high frequencies refer to the densest parts of the H II regions, we expect that $T_e \approx T_e^*$. The [O III] lines are also formed in these regions, and one can compare electron temperatures obtained from optical and radio measurements. There is a very good agreement of these values (Pauls and Wilson, 1977; Walmsley, 1980), at least for Orion, for which large amounts of high quality data are available. This agreement gives one confidence that the values of T_e^* , obtained from high frequency radio lines, are close to the actual electron temperature, T_e .

From surveys of radio recombination lines made at 5 GHz, Churchwell and Walmsley (1975) suggested that the electron temperatures, T_e , of H II regions in the galactic disk increase with distance from the galactic center. Additional evidence in support of this claim was obtained from newer surveys of the H109 α line (Churchwell et al., 1978), H110 α line (Downes et al. 1980), H65/66 α lines (Wilson et al. 1979a, b) and a collection of recombination lines at different frequencies by Mezger et al. (1979). In addition, the surveys of Mezger et al. (1979) and Downes et al. (1980) provided evidence that the H II regions in the Galactic Center region have values of T_e which might be significantly larger than the value obtained from an extrapolation of the gradient found in the disk population of H II regions. However, the Electron Temperatures of Downes et al. probably are too large since the thermal and non-thermal background radiation is included in the continuum temperature estimate. Objections to the interpretation of these results (see e.g. Brown et al., 1978) were based on the following ideas:

(1) The non-LTE masering effects in the line formation process mimic a gradient in T_e^* (which was assumed equal to T_e). This is because the more distant H II regions must have a larger emission

Send offprint requests to: J. E. Wink

Table 1

Table 1

Galactic coordinates l, b	R.A. (1950.0), DEC.	Peak flux density [Jy]	θ_a [']	Source size θ_s [']	Line to Con- tinuum Ratio T_L/T_C	Full width to Half Power $\Delta V_{1/2}$ [km s ⁻¹]	Radial Velocity V_{LSR} [km s ⁻¹]	T_e^* [K]	D_{SUN} [kpc]	$D_{G,C}$ [kpc]	Number of Independent measurements	Log N_c'	Remarks
359.28	17 41 42.8 -29 39 57"	0.5	1.5	1.4	0.28 ± 0.03	25.1±3.0	- 0.2±1.2	800	4.8/15.2	5.2	1	48.5/49.5	
359.43	17 41 25.4 -29 26 58	1.2	<2.2	<2.2	0.15 ± 0.01	35.7±3.0	- 65.7±11.3	6900±	10	0.1	2	49.8	
0.09	17 42 35.0 -28 49 35	≤ 1.4	complex	complex	0.15 ± 0.03	40.0±3.0	- 25.4±11.9	≥ 6600±	10	0.1	2	49.2	$T_e^*(R) = 7300±2200$
0.18	17 43 03.8 -28 47 11	≥ 1.6	<3.5	<3.5	0.06 ± 0.01	59.1±2.3	24.5±0.2	≥ 8800±	10	0.1	4	50.1	$T_e^*(R) = 9500$
0.51	17 43 51.0 -28 31 50	~ 2.0	complex	complex	0.20±0.033	29.8±1.8	45.8±0.9	5900±	10	0.1	4	~50	$T_e^*(R) = 9400±2000$
0.51	17 43 49.6 -28 30 00	~ 1.5	complex	complex	0.26 ± 0.03	24.3±3.3	47.1±0.5	5800±	10	0.1	4	~50	$T_e^*(R) = 10400±3300$
0.60	17 44 04.4 -28 26 00	≤ 2.6	complex	complex	0.127±0.007	37.8±2.0	51.8±0.8	≥ 7100±	10	0.1	1	~50	$T_e^*(R) = 7500±1500$
0.64	17 44 12.3 -28 24 30	≤ 3.1	complex	complex	0.170±0.034	40.0±2.0	60.0±0.7	≥ 5500±	10	0.1	1	~50	
0.67	17 44 10.7 -28 22 17	512.4	1.1	1.7	0.110±0.010	38.7±0.4	65.2±1.0	≥ 7700±	10	0.1	3	50.4	SCR B2 $T_e^*(R) = 7600±1000$
1.13	17 45 30.0 -28 01 01	1.6	1.4	1.4	0.265±0.019	23.0±1.1	- 19.9±0.5	5900±	10	0.2	2	49.5	
3.34	17 50 35.1 -26 05 36	0.7	<1.2	<1.2	0.205±0.019	24.7±2.6	8.0±1.1	6900±	17	7.4	1	49.5	
5.48	17 55 59.0 -24 20 48	0.7	1.3	1.3	0.227±0.026	20.8±2.2	28.3±0.9	7100±	1000	4.6	1	49.4	
5.88	17 57 27.2 -24 03 59	6.3	1.0	1.0	0.061±0.007	62.4±2.1	8.6±2.4	8500±	900	2.6	1	48.7	
5.91	17 57 38.4 -24 03 58	1.5	--	--	0.291±0.030	20.0±0.2	8.2±0.6	6000±	900	2.6	1	48.1	
6.55	17 57 47.0 -23 20 30	1.3	1.4	1.3	0.242±0.016	21.0±1.5	13.2±0.6	6700±	600	17	1	49.9	$T_e^*(R) = 8500±1200$
7.47	17 59 11.6 -22 27 55	1.4	1.1	1.1	0.116±0.010	30.4±0.8	- 16.0±2.0	9200±	1300	27 / 6.2	2	48.9/50.1	velocity shares that of
8.14	18 00 00.4 -21 48 17	2.5	1.3	1.3	0.222±0.010	28.3±1.5	22.1±0.6	5600±	400	4.2/15.6	1	49.0/50.2	" 3 kpc arm"
8.67	18 03 18.4 -21 37 55	1.2	<1.3	<1.3	0.179±0.015	30.3±2.8	42.7±1.1	6700±	900	6	1	48.8	
10.16	18 06 26.6 -20 19 50	6.1	<3	conf.	0.219±0.005	29.2±1.0	12.5±0.3	5500±	200	3.8	2	50.0	W31A
10.32	18 06 01.1 -20 05 48	2.3	conf.	conf.	0.181±0.009	27.5±1.4	12.2±0.9	6800±	500	6	2	49.3	W31B
10.62	18 07 31.7 -19 56 44	4.7	1.0	1.1	0.160±0.008	28.1±1.0	0.3±0.3	7500±	500	6	2	49.4	W31C
12.81	18 11 18.0 -17 56 32	18.0	1.1	1.1	0.189±0.010	32.8±2.3	36.1±0.3	5900±	200	4.5 adopted	2	49.7	W33
13.19	18 11 10.6 -17 29 33	0.8	1.5	2.1	0.296±0.024	18.4±1.6	54.6±0.6	6400±	700	5.8	1	49.1	
13.88	18 11 42.7 -16 46 32	2.5	1.1	1.1	0.278±0.014	21.1±0.5	51.2±0.4	6000±	300	5.4/13.9	2	49.1/49.9	
14.00	18 13 26.9 -16 51 50	0.4	2.5	2.5	0.323±0.048	20.2±1.5	35.2±1.3	5500±	800	4	2	48.5	
15.03	18 17 34.0 -16 13 51	21.4	2	3	0.173±0.005	29.0±0.5	15.8±0.2	6900±	300	2.1	2	49.7	H17
18.14	18 22 12.4 -13 17 41	1.4	1.7	1.7	0.240±0.022	23.0±1.5	53.0±1.3	6300±	700	4.5	2	49.0	S53
18.30	18 22 53.4 -13 12 00	1.0	1.0	1.0	0.232±0.019	31.2±3.2	33.7±1.3	5100±	600	3.0	2	48.2	
20.73	18 25 25.0 -11 31 00	0.9	<1.1	<1.1	0.196±0.027	25.0±2.3	41.6±1.0	6900±	700	6.3	1	48.3	
23.42	18 32 00.2 -08 35 44	~ 0.7	<3.3	<3.3	0.196±0.027	23.4±2.3	55.6±1.0	7100±	900	13.8	2	50.2	
23.71	18 31 09.6 -08 09 51	0.9	1.3	1.3	0.228±0.037	24.2±2.7	103.6±1.1	6300±	1300	9	1	49.8	
23.96	18 31 41.9 -07 57 06	1.4	1.1	1.1	0.235±0.017	20.4±1.7	105.8±0.7	7100±	1000	9	1	49.2	
24.47	18 31 27.2 -07 20 33	2.1	1.3	1.3	0.227±0.013	30.7±1.8	79.2±1.7	5100±	400	6/12	1	49.0/49.6	
24.68	18 34 09.9 -07 27 29	0.8	1.6	1.4	0.202±0.007	29.9±1.1	101.7±0.4	5800±	200	9	2	49.5	
24.81	18 33 29.0 -07 13 50	0.9	1.6	1.4	0.293±0.025	20.7±2.1	112.3±0.9	5800±	700	9	1	49.3	
25.38	18 35 33.4 -06 50 45	3.4	1.3	1.9	0.336±0.024	22.4±1.6	109.5±0.7	4900±	400	9	1	49.4	
25.40	18 34 49.0 -06 43 51	0.5	1.4	1.4	0.147±0.041	29.8±8.0	- 12.3±3.0	6000±	200	13.5	1	50.3	3C385
25.70	18 35 23.0 -06 28 05	0.3	1.7	1.7	0.302±0.061	16.8±3.2	52.7±1.3	7600±	2000	18.5	1	49.6	
25.77	18 34 52.5 -06 19 16	0.5	1.9	<1.6	0.329±0.036	21.8±2.6	110.3±1.1	6700±	1700	14	1	49.7	
26.54	18 35 36.0 -05 32 37	0.9	1.3	1.3	0.188±0.008	30.8±2.8	88.4±1.1	6000±	800	6.6/11.3	1	49.1	
												48.9/49.3	

Table 1

Galactic Coordinates l [$^\circ$]	b [$^\circ$]	R.A. (1950.0) [h:m:s]	DEC. [$^\circ$]	Peak Flux density [μ Jy]	θ_d [$''$]	Source Size θ_s [$''$]	Line to Con- tinuum Ratio $T_{\text{L}}/T_{\text{C}}$	Full Width to Half Power $\Delta V_{1/2}$ [km s $^{-1}$]	Radial Velocity V_{LSR} [km s $^{-1}$]	T_{e}^* [K]	D_{SUN} [kpc]	D_{GC} [kpc]	Number of Independent measurements	Log N c	Remarks
27.28	+0.15	18 37 54.5	-05 00 42	0.7	1.1	1.1	0.190 \pm 0.012	23.0 \pm 2.6	34.8 \pm 0.8	7700 \pm 900	2.6/15.2	7.8	2	47.8/49.4	
27.49	+0.19	18 38 09.7	-04 48 07	0.5	1.6	2.9	0.212 \pm 0.036	27.1 \pm 4.8	32.6 \pm 1.9	5800 \pm 1300	15	7.7	1	49.8	
28.80	+0.17	18 40 38.4	-03 38 49	0.9	1.3	1.4	0.254 \pm 0.024	23.0 \pm 2.4	108.6 \pm 1.0	7100 \pm 700	8.8	4.8	2	49.1	S64, W40
28.9	+3.5	18 28 51.0	-02 07 30	0.9	5.6	5.1	0.204 \pm 0.021	23.6 \pm 3.1	1.1 \pm 1.2	8000 \pm 1400	0.1	10	2	46.5	
29.94	-0.04	18 43 32.4	-02 44 40	1.6	\approx 2	conf.	0.206 \pm 0.017	29.2 \pm 2.4	102.1 \pm 0.9	5800 \pm 600	9	5.1	1	49.8	
30.54	+0.02	18 44 22.9	-02 10 50	0.9	1.0	1.0	0.161 \pm 0.015	29.0 \pm 2.3	45.7 \pm 1.0	7000 \pm 800	13.8	7.2	1	49.5	
30.78	+0.03	18 45 00.4	-01 59 16	6.3		complex	0.160 \pm 0.004	33.5 \pm 0.7	91.0 \pm 0.4	6500 \pm 200	7	5.5	2	50.6	W43
31.40	-0.26	18 46 58.6	-01 32 27	0.5	\approx 2.5	\approx 2.5	0.167 \pm 0.028	30.4 \pm 6.1	81.6 \pm 2.4	6700 \pm 1500	7	5.5	1	49.2	
31.41	+0.31	18 44 59.9	-01 16 06	0.8	\approx 1.0	\approx 1.0	0.314 \pm 0.019	22.0 \pm 1.4	101.5 \pm 0.6	5400 \pm 400	8.5	5.2	1	49.0	
32.80	+0.39	18 47 57.4	-00 05 31	3.6	1.0	1.0	0.158 \pm 0.009	28.3 \pm 2.3	16.4 \pm 1.1	7200 \pm 600	15.6	9.0	2	50.1	
33.91	+0.11	18 50 17.3	+00 51 45	0.8	1.0	1.0	0.218 \pm 0.016	25.2 \pm 1.9	101.7 \pm 0.8	6300 \pm 600	8.2	5.6	1	48.9	
34.26	+0.15	18 50 47.3	+01 10 56	6.7	1.4	1.3	0.168 \pm 0.004	24.1 \pm 0.5	53.8 \pm 0.2	8100 \pm 200	3.7	7.2	2	49.3	
35.19	-1.75	18 59 15.0	+01 08 38	6.5	1.3	1.4	0.195 \pm 0.012	24.2 \pm 0.7	47.3 \pm 0.2	7500 \pm 400	3.2	7.6	2	49.2	
37.54	-0.11	18 57 46.5	+03 58 58	0.6	1.6	1.2	0.221 \pm 0.030	26.0 \pm 2.0	48.3 \pm 0.8	6100 \pm 800	12	7.3	1	49.1	
37.76	-0.22	18 58 33.1	+04 07 41	1.2	1.4	1.4	0.200 \pm 0.017	19.8 \pm 1.6	66.0 \pm 0.7	8300 \pm 900	4.3/12	7.1	3	48.8/49.8	
37.87	-0.40	18 58 24.5	+04 08 21	3.7	1.0	1.0	0.138 \pm 0.006	42.0 \pm 1.9	58.7 \pm 0.6	6000 \pm 400	12	7.1	2	49.7	
42.43	-0.26	19 07 25.8	+08 14 31	0.5	\approx 1.6	\approx 1.5	0.160 \pm 0.025	22.4 \pm 3.5	65.6 \pm 1.6	9000 \pm 2000	5.3/9	7.1	1	48.6/49.0	W49
43.17	+0.00	19 07 51.8	+09 01 20	15	1.6	1.3	0.150 \pm 0.004	30.8 \pm 0.6	6.3 \pm 0.2	7400 \pm 300	14	9.5	3	50.8	
43.23	-0.05	19 08 10.5	+09 03 02	0.6	\approx 1.6	conf.	0.214 \pm 0.023	20.1 \pm 2.1	10.5 \pm 0.8	7800 \pm 1200	0.6/13.9	9.5	1	46.6/49.3	
45.13	+0.14	19 11 06.8	+10 48 30	4.6	1.1	1.2	0.122 \pm 0.026	45. \approx 3.3	58.5 \pm 0.8	6600 \pm 2500	9.5	7.5	2	49.9	
45.45	+0.06	19 12 00.0	+11 03 55	3.5	1.3	1.3	0.171 \pm 0.012	27.3 \pm 0.7	55.5 \pm 0.3	7200 \pm 500	9.7	7.7	1	49.9	
45.48	+0.13	19 11 47.5	+11 07 10	1.3	1.1	1.1	0.180 \pm 0.020	29.4 \pm 1.1	55.7 \pm 0.8	6600 \pm 900	9.7	7.7	2	49.3	
48.60	+0.04	19 18 07.6	+13 49 45	1.0	2.4	2.4	0.183 \pm 0.016	26.0 \pm 2.0	20.8 \pm 0.8	7300 \pm 700	12	9.2	1	50.0	
48.93	-0.29	19 19 58.0	+13 57 40	1.9	1.6	\approx 1.8	0.180 \pm 0.043	30.5 \pm 1.5	66.0 \pm 0.8	7100 \pm 1700	6.6	7.5	2	49.8	
49.08	-0.38	19 20 35.2	+14 03 16	1.1	1.8	1.4	0.206 \pm 0.013	30.6 \pm 2.2	75.6 \pm 0.9	5600 \pm 500	6.6	7.6	1	49.3	
49.20	-0.35	19 20 43.6	+14 10 50	3.7	<1.7	conf.	0.171 \pm 0.006	30.2 \pm 1.0	69.1 \pm 0.4	6600 \pm 400	6.6	7.6	1	49.8	
49.38	-0.30	19 20 55.0	+14 20 55	4.6	1.4	1.4	0.186 \pm 0.006	29.4 \pm 0.9	55.4 \pm 0.4	6300 \pm 300	7	7.9	1	49.7	
49.49	-0.38	19 21 24.4	+14 24 40	26.	1.3	1.4	0.174 \pm 0.010	30.7 \pm 1.1	57.2 \pm 0.1	6500 \pm 400	7	7.9	2	49.8	
49.58	-0.38	19 21 37.0	+14 29 42	1.2	1.4	1.3	0.212 \pm 0.014	30.9 \pm 2.3	61.7 \pm 0.9	5500 \pm 500	6.6	7.6	1	49.0	
55.12	+2.42	19 22 20.0	+20 41 37	0.4	1.0	1.0	0.115 \pm 0.035	45. \approx 9.	-78. \approx 4.	6600 \pm 2200	19.3	15.8	1	49.2	S83A
70.29	+1.60	19 59 51.2	+33 24 33	6.1	1.0	1.0	0.099 \pm 0.007	35.9 \pm 1.2	-24.6 \pm 0.4	9100 \pm 700	9	11	1	49.7	K3-50
70.33	+1.59	19 59 59.0	+33 25 50	2.8	1.0	1.0	0.153 \pm 0.009	28.8 \pm 1.5	-19.7 \pm 0.7	7600 \pm 500	9	11	2	49.4	OH-3
79.30	+1.30	20 26 22.5	+40 02 02	1.6	1.8	2.3	0.145 \pm 0.006	33.7 \pm 2.5	-37.6 \pm 0.8	6900 \pm 700	8.6	11.9	1	49.8	DR7
80.3	+0.8	20 32 07.0	+41 12 40	0.6	1.5	1.4	0.131 \pm 0.022	26.2 \pm 3.0	-63.4 \pm 1.2	9500 \pm 1700	11	13.6	1	49.2	
81.68	+0.54	20 37 14.2	+42 09 05	17.6	1.1	1.1	0.133 \pm 0.011	33.8 \pm 0.4	-0.6 \pm 0.2	7600 \pm 200	1.5	9.9	11	48.7	DR21
108.19	+0.58	22 47 30.7	+59 39 08	1.4	1.2	1.2	0.167 \pm 0.021	25.3 \pm 2.1	-57.1 \pm 0.8	8100 \pm 500	6.0	13.1	2	48.9	S146
108.76	-0.95	22 56 37.0	+58 30 55	0.8	1.0	1.0	0.136 \pm 0.009	26.2 \pm 2.3	-50.1 \pm 0.9	9100 \pm 900	5.2	12.7	1	48.4	S152
110.11	+0.05	23 03 04.0	+59 58 25	1.5	1.1	1.1	0.124 \pm 0.013	44. \approx 6.	-49.8 \pm 1.8	6400 \pm 1000	5.2	12.8	1	48.7	S156
111.54	+0.78	23 11 37.0	+61 11 59	1.9	1.0	1.0	0.125 \pm 0.007	28.8 \pm 2.2	-62.3 \pm 1.4	9000 \pm 1000	2.4 adopted	11.1	1	48.5	NGC7538 OH
111.62	+0.37	23 13 23.2	+60 50 56	0.6	51.1	51.1	0.198 \pm 0.031	22.4 \pm 3.4	-67.5 \pm 1.4	7600 \pm 1300	6.8	14.0	1	48.5	S159
133.71	+1.21	02 21 56.0	+61 52 42	20.1	51.4	1.1	0.163 \pm 0.007	27.5 \pm 0.2	-39.1 \pm 0.1	7600 \pm 300	3.1	12.4	2	49.5	W3A
150.6	-0.9	03 59 29.8	+51 10 38	0.9	1.6	2.5	0.128 \pm 0.010	27.0 \pm 1.5	-24.3 \pm 1.5	9500 \pm 500	3.3 adopted	12.9	3	48.8	S206
151.61	-0.24	04 07 19.7	+51 01 58	0.8	\approx 3.1	\approx 3.0	0.102 \pm 0.010	30.3 \pm 2.0	-49.6 \pm 3.1	10400 \pm 1000	7.6	17	4	49.7	S209

measure (E.M.) in order to be detected. This large value of E.M. favors a larger amplification of radio recombination lines, leading to a lower value of T_e^* .

(2) The H II regions in the inner parts of the Galaxy, ~ 5 kpc from the Sun, are of an intrinsically different type from H II regions near the Sun. Hence a comparison of T_e (or T_e^*) for these different sources is invalid.

The advantages of using the H76 α line are:

(1) Collisional broadening and recombination line masering effects should be negligible. Also deviations from non-LTE in the level populations should be small for the dense H II regions selected at high frequencies.

(2) At three times the frequency of the H110 α line, the angular resolution of our telescope will be one-third, but the H112 α and H110 α survey source lists could be used as a starting point for our survey. At 23 GHz, for example, a new galactic plane continuum survey would be required to produce a source list.

(3) The confusion effect of the extended galactic background will be smaller than at lower frequencies.

(4) The atmospheric effects will be smaller than at higher frequencies.

Sources in the galactic longitude range 359° to 55° were taken from the H110 α survey (Downes et al., 1980). Most of these sources are located within 10 kpc of the Galactic Center. In order to extend the source sample to the outer parts of the Galaxy, we also selected H II regions from the H112 α survey of Wink et al. (1983).

2. Observations

The observations were made in Nov. 1981 from the prime focus of the 100-m telescope of the MPIFR. At the rest frequency of the H76 α line, 14.7 GHz, the full width to half power (FWHP) of the telescope beam is $1'$. The receiver was a single-channel, three stage cooled parametric amplifier; the system noise was 150 K to 180 K at the elevations where our measurements were made. The spectrometer was an autocorrelator, used as two parallel 192 channel receivers. The velocity resolution was 1.3 km s^{-1} and the total analyzing band covered 204 km s^{-1} . In order to reduce the system noise, there was no Dicke switch in the system; hence both line and continuum measurements were carried out using the total power output of this receiver. In all cases, spectra were at the position of the continuum peak, which was determined immediately prior to the line measurements by cross scans measured over an angular distance of $6'$. An additional continuum measurement was made afterwards. This procedure was adopted to minimize systematic errors in the determination of the electron temperature. The line measurements were made employing position switching, the reference position was five minutes of time east to the peak position. Each spectral line measurement consisted of a 5 min integration on-source, followed by a 5 min integration on the reference. This cycle was repeated twice. In some cases, this sequence was repeated.

The ratio of the integrated H76 α line to the continuum intensity is required for the determination of T_e^* [in Column (11) of Table 1]. The line emission is assumed to arise *only* from the discrete source, and *not* from the extended background. Then, to determine the continuum intensities, we have taken the zero level at an angular distance of up to $6'$ (depending on source size) from the center position. For sources in our survey outside the Galactic Center, the background continuum is weak (typically $\lesssim 10\%$)

relative to the peak intensity of the discrete source, and the effect of any thermal continuum background (which might contribute to the line) is negligible. This is *not* the case in the Galactic Center region. In order to investigate the effect of this background emission on the line observations, we have measured, in a few cases, reference spectra at positions surrounding the discrete source. These cases will be discussed individually in the appendix. In general, the off-peak spectra near the Galactic Center show H76 α emission at radial velocities close to that of the discrete source. For these objects, some of the background emission is thermal, and the continuum intensity, derived from the cross scans is too small. Thus T_e^* should be raised. No correction can be made from continuum results alone, since we have not measured these relative to a position off the galactic plane. In order to estimate a correction, we derive a corrected integrated H76 α line emission from $(\int T_L(\text{peak})dV - \int \bar{T}_L(\text{offsets})dV)$, the difference between the on and off-source contributions. Combining this difference with the measured continuum temperature of the discrete source, we derive the corrected electron temperatures, $T_e^*(R)$, in the notes in Table 1. These are presumably more appropriate for the discrete sources.

3. Results

We collect our observational results in Table 1: the galactic coordinates, the equatorial coordinates (epoch 1950.0), the source peak flux density, the observed source size (i.e. including the $1'$ telescope beam), the H76 α line-to-continuum ratio, full width to half power and radial velocity of the H76 α line obtained from gaussian fits, T_e^* , heliocentric and galactocentric distances, number of independent observations of a source, and the number of ionizing photons, N'_c (from the distance to the sun and the integrated flux density). Only linear baselines have been subtracted from our spectra. The errors which we quote for T_e^* have been determined from gaussian fits to the H76 α line data and the scatter in the peak intensities from continuum cross scans. Results on different days were combined using a weighted mean. Values of T_e^* are calculated with the observed ionized helium abundance y^+ , or if unknown for $y^+ = 0.08$.

The distance estimates were taken from the H110 α survey of Downes et al. (1980) and from Wink et al. (1982) or are derived from a rotational model with a constant circular velocity of 250 km s^{-1} outside the solar circle. There are some doubtful distance estimates; these are indicated in the Notes.

4. Discussion

Comparison with other surveys

In Fig. 1 we show the differences between our values of T_e^* and those derived in other recent surveys. Evidently, the largest scatter occurs in the H110 α survey of Downes et al. (1980). This is probably caused by the inclusion of background emission in the continuum temperatures and by the observational procedure: in contrast to later surveys, the H110 α line and corresponding continuum measurements were not made together, and pointing difference make the T_e^* (H110 α) results rather uncertain. In contrast, a comparison with previous H76 α results and H65/66 α measurements (Wilson et al., 1979a, b; Thum et al., 1980; Mezger, et al., unpublished) show a smaller scatter. There is however a small residual offset in the differences of T_e^* values; this may be

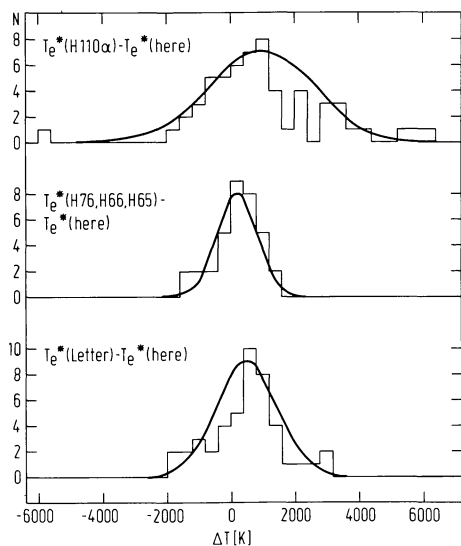


Fig. 1. Histograms of the differences in the values of LTE electron temperatures, T_e^* , for sources common to other recent surveys and this survey. The H110 α (Downes et al., 1980) and this survey have 58 sources in common. The difference between T_e^* values is 980 ± 2000 K. (The uncertainty is the rms scatter about the mean difference.) The H65 α , H66 α , and H76 α surveys (Wilson et al., 1979a, b and unpublished) and this survey have 34 sources in common. The difference in T_e^* values is 200 ± 700 K. The T_e^* values from Mezger et al. (1979) (referred to as “Letter”) are the best estimates from results for sources observed in the H110 α , H90 α , H76 α , and H66 α lines with the 100-m telescope. There are 45 sources in common with this survey; the differences in T_e^* values is 500 ± 1100 K

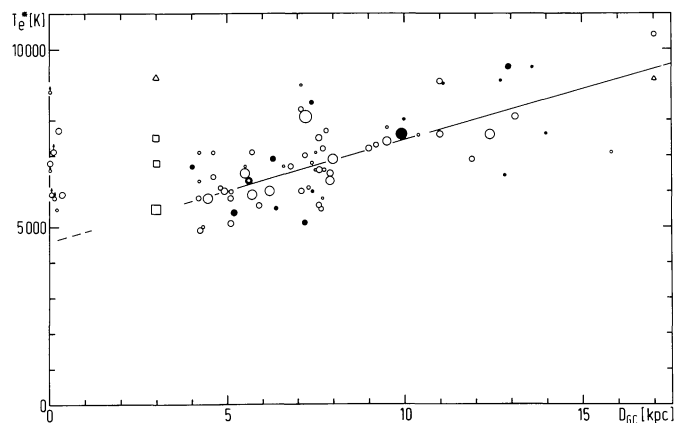


Fig. 2. A plot of T_e^* versus distance from the Galactic Center, D_{GC} . The larger dots represent sources with more accurate values of T_e^* ; the small dots are those with less accurately determined values of T_e^* , and should be given lower weight. The three open squares are sources in the W31 complex. Because of non-circular motions, these sources may be located in the “3 kpc” arm. The open triangles represent G 7.47 + 0.06. This source has a negative radial velocity, and might be either 4 or 17 kpc from the Galactic Center, depending on whether the motion has a large non-circular component or not. Open symbols indicate $N'_C \geq 10^{49} \text{ s}^{-1}$, filled symbols $N'_C < 10^{49} \text{ s}^{-1}$. The solid line is the result of a weighted, least-squares linear fit to the data for sources between 4 and 17 kpc. We indicate the extrapolation of this result to the sources in the Galactic Center by a dashed line

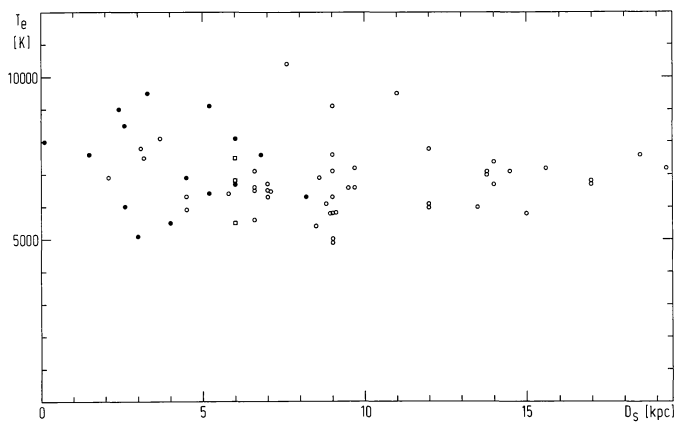


Fig. 3. A plot of T_e^* versus distance from the Sun, D_S . Symbols have the same meaning as in Fig. 1. The W31 sources, the GC sources and 9 sources with unresolved distance ambiguity are omitted. They would complicate the picture but not affect our conclusion. There is no dependence of T_e^* on D_S , although there is strong dependence on D_{GC} (in Fig. 2). Taken together, these two results imply that the variations in T_e^* are not related to distance from the Sun, but to distance from the Galactic Center

caused by our assumption that, where no measurements are available, the abundance of ionized Helium is 0.08, compared with a value of 0.05 used in the earlier results. For $T_e^* = 8000$ K, this increase in y^+ will cause a decrease of 200 K or 2.5%. Overall, different recombination lines measured at frequencies higher than 14 GHz agree well. One might believe that the influence of strong non-LTE effects should cause T_e^* from different lines to be different. The good agreement we observe leads us to believe that non-LTE effects are effectively small over the range of frequencies from 5 to 22 GHz.

Electron temperature gradients

In Fig. 2, we plot our T_e^* values versus distance from the Galactic Center, D_{GC} . A gradient is definitely present. In Fig. 3, we plot T_e^* against distance from the Sun. If the variation in T_e^* were caused by effects related to distance from the Sun, Fig. 3 would also show a gradient. Since there is none, we conclude that there is a real gradient in T_e^* with D_{GC} . Shaver (1980) shows that $T_e = T_e^*$ for $\nu = 0.081 \text{ EM}^{0.36}$, i.e. for $\nu = 14.7$ GHz, the Emission Measure, EM, is $\sim 2 \cdot 10^6 \text{ pc cm}^{-3}$. Correcting for beam dilution, the sources in our sample have $10^5 < \text{EM} < 10^7 \text{ pc cm}^{-6}$ based on our continuum data. Most of the low EM sources are extended; but are probably clumped in several higher EM regions. Thus our values are approximate, and detailed results require high resolution measurements with interferometers. Using the deconvolved sizes and EMs, we find that the high EM sources ($> 10^6 \text{ pc cm}^{-6}$) also have densities larger than $5 \cdot 10^2 \text{ cm}^{-3}$. Following the procedure of Wilson et al. (1979a), we have applied a homogeneous sphere model calculation to our data, to calculate the electron temperature, T_e . On the average, T_e is less than T_e^* by 10%. Only 2 sources have $T_e \leq 0.8 T_e^*$, while only 3 sources have $T_e \geq 1.2 T_e^*$. These sources are not concentrated at any single galactocentric distance. These corrections cannot be considered very accurate for an individual source, because detailed models of the distribution of electron density and EM would be required. However, high

resolution, high frequency surveys such as ours certainly give more realistic estimates of T_e than those obtained from lower frequency line and continuum data, which tend to underestimate the EM. We believe that on the average our corrections are valid. For our results, the gradient in T_e^* represents a very similar gradient in T_e . Previous surveys of recombination lines at lower frequencies showed a flatter gradient of T_e vs. D_{GC} , because of non-LTE effects. Previous high resolution surveys at $\nu > 10$ GHz showed results similar to ours, but had only a limited sample of sources (see Table 2). Our contribution to this discussion is the more than twofold increase of the number of sources with measurements at frequencies where line masering is small. In Figs. 2 and 3, we also differentiate between H II regions which have a Lyman continuum photon flux N'_c greater or less than 10^{49} . H II regions with $N'_c > 10^{49} \text{ s}^{-1}$ require a star earlier than 06.5 for their excitation. We see no difference between these two groups of sources, and conclude that the value of N'_c has little effect on the gradient of T_e with D_{GC} in our sample. Also we find no dependence of T_e^* on electron density, N_e . This might be because estimates of N_e are considerably more uncertain, because of the role of source size and clumping. From the data presented in Figs. 2 and 3, we conclude that there is a gradient in T_e in the galactic disk, from 4 to at least 12 kpc from the Galactic Center. Our results include 13 sources outside the Solar circle. This is the largest collection of such sources in the outer part of the Galaxy, and thus puts the discussion of any T_e gradient there on a better statistical basis. Our T_e^* values in the range $D_{GC} = 11\text{--}17$ kpc definitely rise with D_{GC} , indicating that the increase between 4 and 12 kpc continues at larger galactocentric distances.

We have fitted our data for sources between 4 and 17 kpc using a linear function. The result is listed in Table 2, where for comparison, we list the T_e^* gradients from other recombination line surveys. With one exception, the fits were linear, and we simply give the published results. The relation given by Mezger et al. (1979) involved a logarithmic function; we have made a linear fit to the data for the purposes of comparison. The values from

various surveys agree rather well. Our gradient is marginally ($\sim 5\%$ – 10%) flatter than those in surveys done at 5 GHz. We believe that our data are less influenced by non-LTE results, and are to be preferred.

In making the fit, we have excluded the H II regions in the Galactic Center, and the sources with $D_{GC} = 3.5$ kpc. The case for excluding the Galactic Center (G.C.) sources is based on the observation that there are few H II regions within 3.5 kpc of the GC (except those in the GC itself). One interpretation is that the evolution of and physical conditions in the GC are very different from the disk (see Oort 1977 for a discussion). The extrapolation from our fit to the GC shows that the average observed T_e of these sources is ~ 2000 K larger than predicted from our fit to data in the disk. This behavior was reported for the results collected by Mezger et al. (1979) and the H110 α survey (Downes et al., 1980). Our larger sample establishes this fact more convincingly. At lower frequencies this effect, especially for the H110 α survey, could have been caused by the inclusion of a large amount of non-thermal background in the continuum intensity of the sources, since the zero of the continuum level in the H110 α survey was taken with respect to a position well away from the galactic plane. This background would contribute to the continuum, but not the line, emission, thus mimicking sources with high values of T_e . This effect is smaller in the H76 α survey, since the relative proportion of non-thermal emission should be less. Also, we have reduced the influence of the background emission by taking the zero level of the continuum with respect to the end points of the continuum cross scans (see Notes to the Individual Sources and Figs. 3 and 4). Our analysis of the H76 α data and the agreement of our results with other surveys leads us to conclude the effect is real – the T_e 's of GC sources are larger than the extrapolated value.

Scatter in T_e values for disk sources

The unweighted mean value and RMS scatter for the 23 sources between 7 and 8 kpc is 6800 ± 1000 K. The uncertainty is some-

Table 2. Fits to T_e^* vs. D_{GC} for H II regions in the disk

Recombination line transition used	No. of sources	Relation obtained	Correlation coeff.	Ref.
H110 α	133	$4600 + 340 D_{GC}^a$	0.320	Downes et al. (1980)
H109 α	33	$\begin{cases} 5081 + 252 D_{GC}^a \\ 4425 + 315 D_{GC}^b \end{cases}$	0.673	Churchwell et al. (1977) Excluding source G10.6–0.4 from data in their Fig. 3
H137 β	30	$\begin{cases} 5534 + 250 D_{GC}^a \\ 4870 + 342 D_{GC}^b \end{cases}$	0.591	Churchwell et al. (1977) Excluding source G10.6–0.4 from data in their Fig. 3
H86 α	19	$4700 + 390 D_{GC}^a$	0.815	Lichten et al. (1979)
H108 β	19	$6000 + 250 D_{GC}^a$	0.375	Lichten et al. (1979)
H76 α	72	$\begin{cases} 4788 + 268 D_{GC}^a \\ 4600 + 285 D_{GC}^b \end{cases}$	0.703	Here, excluding Galactic Center and “3 kpc” sources Here, excluding Galactic Center and “3 kpc” sources, weighted
H109 α + H90 α + H76 α + H65 α	62	$5340 + 270 D_{GC}^a$	0.681	Mezger et al. (1979)
H109 α + H110 α + H76 α	67	$3150 + 433 D_{GC}$	0.79	Shaver et al. (1983)

^a Unweighted fit to data

^b Fit to data weighted by inverse sigma squared

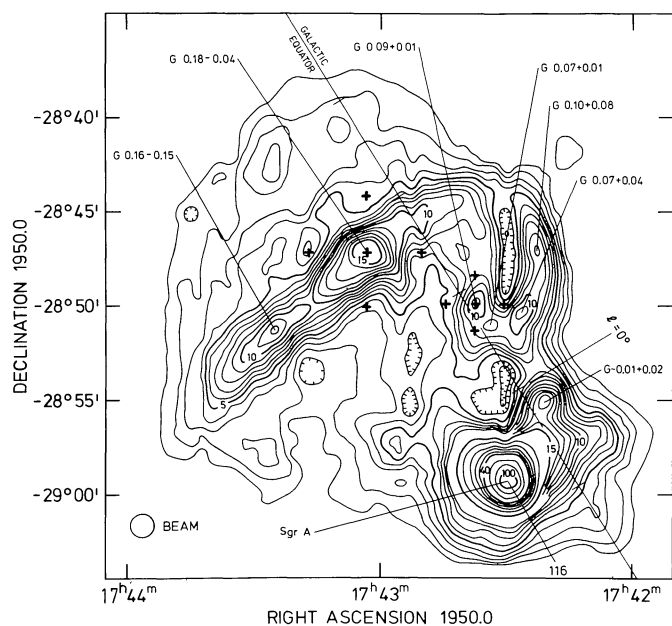


Fig. 4. A continuum map of the Sgr A region made at 10.7 GHz with an angular resolution of 90" (Downes et al., 1978). The thick crosses mark the positions where H76 α spectra were taken

what larger than the measurement uncertainties for the stronger sources. If we restrict our sample to sources with peak flux densities > 1.5 Jy, we have 13 sources; the average T_e^* value is 7000 ± 800 K. Selecting sources from the W51 complex (see Bieging, 1975), we have 6 H II regions with $T_e^* = 6000 \pm 600$ K. The difference between this subset and the whole group is three times the combined standard error. Thus there is no convincing evidence for systematic source-to-source variations. From the group of sources in the 7–8 kpc region, only two, G 5.88–0.41 and G 34.26+0.15, differ from the average value by more than twice the rms.

Relation of T_e values to abundance of “metals”

Churchwell et al. (1978) concluded that changes in the value of T_e^* in H II regions are caused mainly by changes in the abundance of C, N, O (“metals”) relative to Hydrogen. Mezger et al. (1979) have used previously published optical measurements of T_e and the relative abundance of O to H in other galaxies to relate the observed values of T_e^* in our galaxy into a (O/H) ratio. Applying this conversion to our data we have

$$\log(\text{O}/\text{H}) = -0.055 D_{\text{GC}} - 2.73 \quad \text{for } D_{\text{GC}} \geq 4 \text{ kpc.}$$

That is, (O/H) is $2 \cdot 10^{-4}$ at $D_{\text{GC}} = 17$ kpc [or 30% of the “Cosmic” value given by Allen (1973)] and $1.2 \cdot 10^{-3}$ at $D_{\text{GC}} = 4$ kpc (or twice the “Cosmic” value). A preprint of a combined radio-optical survey in the southern part of the galaxy (Shaver et al., 1983) has come to our attention. They cover a similar range of galactocentric distances and try to obtain T_e from T_e^* . They obtain somewhat different values for the (O/H) ratio: at 4 kpc, namely, (O/H) = $1.2 \cdot 10^{-3}$, and at 17 kpc, (O/H) = $1.6 \cdot 10^{-4}$; the $T_e - D_{\text{GC}}$ results from this survey (done at 5 GHz) are listed in Table 2. The source sample is nearly independent of ours, and the T_e -“Metals”

relation independent of that done by Mezger et al. (1979). In view of these differences, the agreement is encouraging. Values of gradients in the Metals based on optical surveys are summarized by Panagia and Tosi (1980). The sense of these gradients agrees with ours, but the magnitude is larger. Since the range in distance from the Sun for the optical results is relatively small, measurement errors may contribute to the differences.

The sources in the Galactic Center provide the most tantalizing result. If the T_e -Metals relation is applied to the electron temperature of these H II regions, one finds an (O/H) abundance ratio comparable to that near the Solar System. This is somewhat surprising in view of the idea (see e.g. Oort, 1977) that a great deal of nuclear processing in stars has taken place there; such processing is manifested in the ($^{12}\text{C}/^{13}\text{C}$) ratios (see Penzias, 1980). Although there are at present no measurements which contradict the (O/H) ratio we find for the Galactic Center, it is likely that the stellar population distribution in the Galactic Center is markedly different from that in the disk and thus the T_e -metal relation is also different. [The relation between T_e and (O/H) was obtained for H II regions in the disks of a small sample of external galaxies and our Galaxy.] It may be that the Initial Mass Function in the Galactic Center is heavily weighted toward low mass stars. Such objects would produce a great deal of ^{13}C from ^{12}C , but little ^{12}C or ^{16}O from He. [In this context, see the discussion of Lacy (1982).] Direct measurements of the (O/H) ratio should resolve this question.

5. Conclusions

1. Measurements of 84 H II regions in the H76 α line and radio continuum at 14.7 GHz more than double the number of sources with line and continuum measurements at frequencies above 10 GHz. This survey is nearly complete for thermal sources between galactic longitudes 359° and 50° with peak flux densities greater than 2 Jy. Outside the solar circle our survey includes 13 sources; this number is large enough to obtain a reliable trend for the run of electron temperature at large distance from the Galactic Center. Also limited mapping in line and continuum was made for a few sources, mostly in the Galactic Center, where the intensity of the extended continuum background emission was an appreciable fraction of the peak intensity of the discrete source. The line and continuum data were combined to produce LTE electron temperatures, T_e^* .

2. From comparisons with other high frequency radio recombination line surveys and model calculations, the actual electron temperature, T_e , is close to T_e^* , obtained from data at this frequency. As in previous studies, there is an increase of T_e^* with distance from the Galactic Center, D_{GC} , for sources in the disk ($D_{\text{GC}} \geq 4$ kpc). A new result from this survey is that the increase of T_e^* with D_{GC} continues out to distances of 17 kpc. From a least-squares, weighted linear fit, $T_e^* = 4600 + 285 D_{\text{GC}}$; the unweighted fit yields $T_e^* = 4800 + 270 D_{\text{GC}}$. The correlation coefficient is 0.70. The large source sample in the present survey reduces the possibility that selection effects cause the $T_e^* - D_{\text{GC}}$ relation. There is no correlation of T_e^* with distance from the Sun, D_s . Hence the variation in T_e^* is not caused by systematic effects related to D_s .

3. The scatter in T_e^* for disk sources at the same D_{GC} exceeds the noise uncertainties in a few cases; this may be evidence for source-to-source variations. If such variations are present, they are not a large fraction of the value of T_e^* .

4. As in previous studies, T_e^* values for Galactic Center sources (6700 ± 1000 K (RMS scatter)) are significantly larger than 4600–4800 K, the value extrapolated from the data for disk sources. The contributions from this survey to Galactic Center measurements are: (1) the four-fold increase in the number of T_e^* determinations for sources at high frequencies, where non-LTE effects are less important, and (2) partial mapping of some sources, which makes it less likely that the large values of T_e^* are caused by confusion with the extended background emission.

5. In the disk, the gradient in T_e is probably caused by a gradient in the relative abundance of “metals”, such as Oxygen, which control the cooling of H II regions. Using the average relation between T_e and the abundance of Oxygen from Mezger et al. (1979), we obtain for our data a variation in the O/H value of 6 between $4 \leq D_{GC} \leq 17$ kpc; our derived relation is

$$\log(O/H) = -0.055 D_{GC} - 2.73 \quad \text{for } D_{GC} \geq 4 \text{ kpc.}$$

The values of T_e for the Galactic Center sources imply a (O/H) ratio which is close to the Solar System value, if this relation of (O/H) and T_e applies.

Acknowledgements. J.H.B.’s travel to and from the MPIFR, and his stay there during the observing session was supported by NATO Grant 161-80. We thank P. G. Mezger for his encouragement and support of this project, and critical comments about the text. C. M. Walmsley provided valuable advice and access to the computer program which allows estimates of T_e from the line and continuum data.

Appendix. Notes to individual sources

G 359.28–0.26

This source has been placed at the near kinematic distance. However, since it is located near $l=0^\circ$, any small non-circular velocity could cause a large change in the distance.

G 0.09+0.01

This source has a complex structure (see Fig. 4): seemingly compact in α , but extended in δ . At 4 positions (marked by crosses in Fig. 4) offset by $\pm 90''$ in α or δ , respectively, there is an H76 α line similar to the one observed toward the peak. Hence the background contributes appreciably to the line emission from the peak, and the T_e^* in Table 1 is a *lower* limit to the T_e^* from the discrete source.

G 0.18–0.05

There is no appreciable line emission at each of the 4 positions offset by $\pm 180''$ in α and δ , respectively, from the peak (see Fig. 4). However, subtracting the average of the 4 line spectra from the one at the peak lowers the line temperature and reduces the linewidth. Hence the T_e^* in Table 1 must be a lower limit.

G 0.49–0.05 and G 0.51–0.04

The off-peak positions where spectra were taken are shown in Fig. 5. An H76 α line was detected at each off-peak position: the line parameters are similar to those for the peak position. Thus the

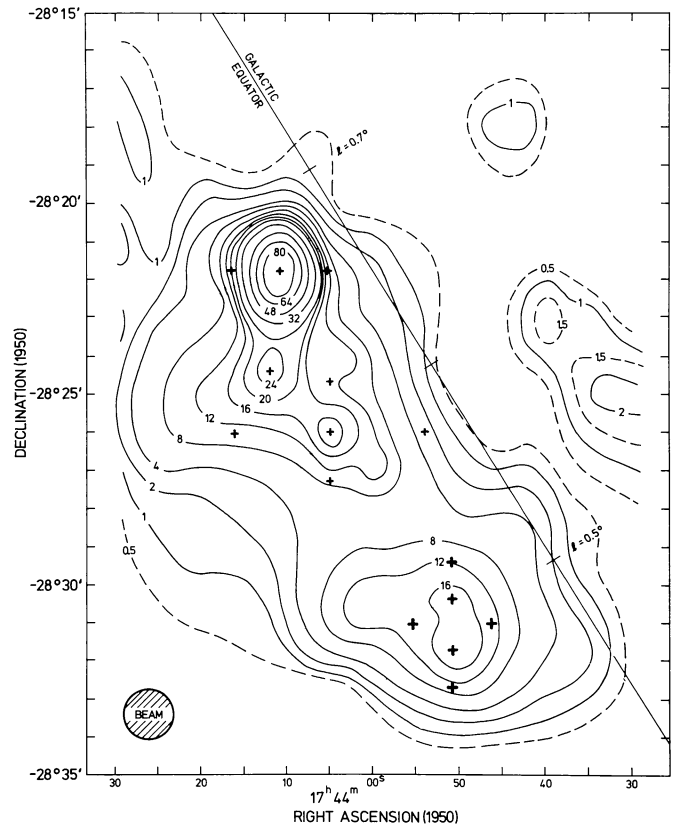


Fig. 5. A continuum map of the Sgr B2 region, made at 10.7 GHz with an angular resolution of $90''$ (Downes et al., 1978). The thick crosses mark positions where H76 α spectra were taken

line emission from the peak includes a contribution from the background, and the value of T_e^* in Table 1 is a lower limit.

G 0.60–0.05 and G 0.64–0.05

These sources are barely resolved by our $1'$ beam. Spectra were taken at off-peak positions shown in Fig. 5. The H76 α line intensity is $\sim 30\%$ of that for G 0.60–0.05; hence the T_e^* values in Table 1 are lower limits.

G 0.67–0.03

See Fig. 5. The continuum source Sgr B2. Spectra were taken at $\Delta\alpha = \pm 75''$ from the peak. Subtracting these line and continuum intensities does *not* appreciably change T_e^* .

G 5.88–0.41

This source shows the broadest line in our survey. Spectra taken at $\Delta\delta = \pm 1'$ have linewidths of $\sim 25 \text{ km s}^{-1}$, but with the same center velocity.

G 5.91–0.43

The continuum intensity was obtained from the α scan through the peak of G 5.88–0.41.

G 10.16–0.35

W31 A, a complicated continuum source; details of the structure are discussed by Martin-Pintado et al. (1983).

G 15.03–0.69

The peak of M17. The H76 α line is flat-topped. This is probably caused by a blending of two velocity features (see Gull and Balick, 1974; Wink et al., 1982).

G 23.42–0.21

A complex source. The continuum scan in δ shows 2 peaks, at $\Delta\delta = \pm 30''$ from the position listed in Table 1.

G 25.70+0.03

The continuum intensity is with respect to a plateau in the α scan.

G 25.77+0.21

Continuum measurement is confused by a source 5' north.

G 28.9+3.5

A nearby H II region. The value of T_e^* may be somewhat underestimated because the source has a large angular size, and the continuum scans may not have reached zero.

G 30.78–0.03

Compact continuum source on a weaker extended background.

G 43.17+0.0

Measurements in the H76 α line at $\Delta\alpha = \pm 1'$ show no difference in T_e^* from the value obtained for the peak.

G 43.23–0.05

Continuum measurement is confused with W49.

G 48.6–0.04 to G 49.44–0.38

Some confusion from weaker continuum sources.

G 55.12+2.42

Weakest line observed in this survey ($T_L = 7$ mK), hence large uncertainties.

G 151.61+0.24

Although a weak line, there is good agreement between the 4 independent determinations of T_e^* .

References

- Allen, C.W.: 1973, *Astrophysical Quantities*, The Athlone Press, London
- Bieging, J.: 1975, in *H II Regions and Related Topics*, eds. T.L. Wilson and D. Downes, *Lecture Notes in Physics* **42**, 443, Springer, Berlin, Heidelberg, New York
- Brockelhurst, M., Seaton, M.J.: 1972, *Monthly Notices Roy. Astron. Soc.* **157**, 179
- Brown, R.L., Lockman, F.J., Knapp, G.R.: 1978, *Ann. Rev. Astron. Astrophys.* **16**, 445
- Churchwell, E., Walmsley, C.M.: 1975, *Astron. Astrophys.* **38**, 451
- Churchwell, E., Smith, L.F., Mathis, J., Mezger, P.G., Huchtmeier, W.: 1978, *Astron. Astrophys.* **70**, 719
- Downes, D., Goss, W.M., Schwarz, U.J., Wouterloot, J.G.A.: 1978, *Astron. Astrophys. Suppl. Series* **35**, 1
- Downes, D., Wilson, T.L., Bieging, J., Wink, J.: 1980, *Astron. Astrophys. Suppl. Series* **40**, 379
- Gärdner, F.F., McGee, R.X.: 1967, *Nature* **213**, 480
- Goldberg, L.: 1966, *Astrophys. J.* **144**, 1225
- Griem, H.: 1967, *Astrophys. J.* **148**, 547
- Gull, T.R., Balick, B.: 1974, *Astrophys. J.* **192**, 63
- Lacy, J.H.: 1982, in *The Galactic Center*, eds. G.R. Riegler and R. Blanford, AIP Conference Proceedings No. 83, AIP, New York, p. 53
- Lichten, S.M., Rodriguez, L.F., Chaisson, E.J.: 1979, *Astrophys. J.* **229**, 524
- Lockman, F.J., Brown, R.L.: 1975, *Astrophys. J.* **201**, 134
- Martin-Pintado, J., Wilson, T.L., Johnston, K.J., Henkel, C., Bieging, J.H.: 1983 (in preparation)
- Mezger, P.G., Höglund, B.: 1967, *Astrophys. J.* **147**, 490
- Mezger, P.G., Pankonin, V., Schmid-Burgk, J., Thum, C., Wink, J.: 1979, *Astron. Astrophys.* **80**, L 3
- Oort, J.H.: 1977, *Ann. Rev. Astron. Astrophys.* **15**, 295
- Panagia, N., Tosi, M.: 1980, *Astron. Astrophys.* **81**, 375
- Pauls, T.A., Wilson, T.L.: 1977, *Astron. Astrophys.* **60**, L 31
- Penzias, A.A.: 1980, *Science* **208**, 663
- Shaver, P.A.: 1980, *Astron. Astrophys.* **91**, 279
- Shaver, P.A., McGee, R.X., Newton, L.M., Danks, A.C., Pottasch, S.R.: 1983, *Monthly Notices Roy. Astron. Soc.* **204** (in press)
- Seaton, M.J.: 1980, in *Radio Recombination Lines*, ed. P.A. Shaver, Vol. 80, *Astrophysics and Space Sci. Library*, Reidel, Dordrecht, p. 3
- Thum, C., Mezger, P.G., Pankonin, V.: 1980, *Astron. Astrophys.* **87**, 269
- Walmsley, C.M.: 1980, in *Radio Recombination Lines*, ed. P.A. Shaver, Vol. 80, *Astrophysics and Space Sci. Library*, Reidel, Dordrecht, p. 37
- Wilson, T.L., Bieging, J., Wilson, W.E.: 1979a, *Astron. Astrophys.* **71**, 205
- Wilson, T.L., Pauls, T.A., Ziurys, L.M.: 1979b, *Astron. Astrophys.* **77**, L 3
- Wink, J.E., Altenhoff, W.J., Mezger, P.G.: 1982, *Astron. Astrophys.* **108**, 227
- Wink, J.E., Altenhoff, W.J., Mezger, P.G.: 1983 (in preparation)